Leading edge vortex control on a delta wing with dielectric barrier discharge plasma actuators

Lu Shen and Chih-yung Wen[a)]
Department of Mechanical Engineering, The Hong Kong Polytechnic University, Kowloon, Hong Kong

(Received xx accepted xx; published online xx)

This paper presents an experimental investigation of the application of dielectric barrier discharge (DBD) plasma actuators on a slender delta wing to control the leading edge vortices (LEVs). The experiments are conducted in a wind tunnel with a Reynolds number of 50 000 based on the chord length. The smoke flow visualization reveals that the DBD plasma actuators at the leading edges significantly modify the vortical flow structure over the delta wing. It is noted that symmetric control at both semi-spans and asymmetric control at a single semi-span leads to opposite effects on the local LEVs. Particle image velocimetry (PIV) indicates that the shear layer is deformed by the actuators. Therefore, both the strength and the shape of the LEV cores are deeply affected. The six-component force measurement shows that the DBD plasma actuators have a limited effect on lift and drag while inducing relatively large moments. This suggests that the DBD plasma actuator is a promising technique for delta wing maneuvering.

Delta wing geometry is a popular configuration for aircrafts due to its good performance in lift generation, stability, and maneuvering. It is well known that a pair of leading edge vortices (LEVs) dominates the flow over a delta wing and generates additional vortex lift. However, vortex breakdown happens on the delta wing at sufficiently high angles of attack, resulting in a loss of lift and stability. In recent decades, many efforts have been devoted to developing methods for LEV control.[1,2] Recently, the applications of dielectric barrier discharge (DBD) plasma actuators for flow control have greatly increased.[3–6] DBD plasma actuators offer the advantages of flexibility, fast response, and efficiency. Several studies on the application of DBD plasma actuators for active flow control over a delta wing have been reported in the past few years.[7–10] However, the underlying control mechanism is still unclear.

The work presented here is a continuation of our previous study, in which we found that asymmetric control (only the DBD plasma actuator on one semi-span is ignited) can significantly modify the global flow structure over a delta wing: the LEV breakdown location at the controlled semi-span is advanced, while that at the uncontrolled semi-span is delayed.[11] Motivated by this observation, a further investigation was conducted to understand the flow physics and the control mechanism.

The experiments were conducted in a closed-circuit low-speed wind tunnel with a test section of 2.4 m (length)-$\times$ 0.6 m (width) $\times$ 0.6 m (height). The turbulent intensity of this facility is less than 0.4%. In our experiments, the free stream velocity is 2.64 ms^{-1}, resulting in in a Reynolds number of $Re = 50\,000$ based on the chord length of the delta wing model. The schematics of the delta wing model used in the experiments are shown in Fig. 1. The wing was made of acrylic and had 75° swept leading edges, a chord length of 280 mm, a root span of 150 mm, and a thickness of 5 mm. The leading edges were beveled to 35° on the windward side to fix the separation points. The model was mounted by a sting on the windward side near the trailing edge. Part of the delta model's surface was milled down to install the DBD plasma actuators so that the actuators were flush with the surface. The electrodes of the actuators were made of copper films with a thickness of 0.025 mm. The widths of the exposed and insulated electrodes were 2 and 20 mm, respectively, and both electrodes were 100 mm long. The dielectric barrier comprised of 10 layers of a 0.06 mm Kapton film. The two pairs of DBD plasma actuators covered from 0.12 c to 0.47 c and from 0.52 c to 0.92 c, respectively. These four DBD plasma actuators could be operated independently. Notably, due to limitations on fabrication when wrapping the DBD actuator sheet around the leading edge, an arc with a radius of less than 1 mm was inevitably present at the tip of the leading edge. In this investigation, the actuators were powered by a sine waveform AC power supply with a 12 kV peak-to-peak voltage and a frequency of 20 kHz. Because the exciting frequency was much higher than the frequencies of the unsteady flow phenomena over the delta wing,[2] the control was regarded as a continuous effect on the flow field.

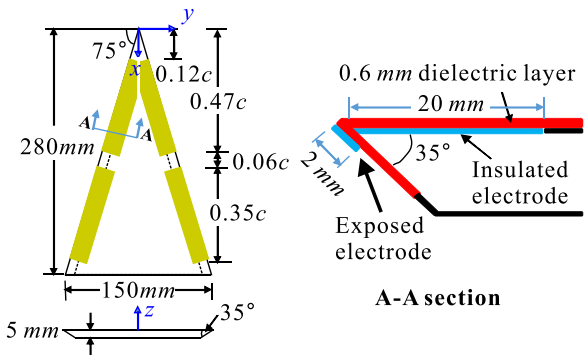

FIG. 1. Schematics of the delta wing model and the configuration of DBD plasma actuators.

[a)]Electronic mail: cywen@polyu.edu.hk

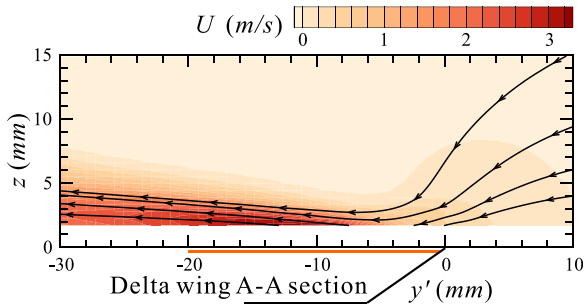

FIG. 2. Time-averaged velocity contour of the ionic wind induced by the DBD plasma actuator at the leading edge in quiescent air.

In the smoke flow visualization experiment, a steel wire (with a diameter of $\phi = 0.8$ mm) coated with olive oil was set about 0.3 m upstream of the delta wing. The oil coating was heated to generate smoke continuously. The flow field was illuminated by a continuous 1 W laser. A Nikon D5200 digital camera was used to capture snapshots with an exposure time of 1/200 s. For the particle image velocimetry (PIV) measurement, the entire wind tunnel was seeded with olive oil droplets generated by using a TSI 9307 aerosol generator. A 532 nm dual-pulse laser (with each pulse of 600 mJ) was used as the light source. The images were acquired by using a CCD camera with a resolution of 1392×1040 pixels. The aerodynamic performance of the delta wing was measured with a load cell (ATI, Nano 43) installed in the supporting sting. To avoid electromagnetic interference, all devices were grounded.

First, the characteristics of the DBD plasma actuators were determined by the PIV measurement. Figure 2 shows the time-averaged velocity contour (in the A-A section) of the ionic wind induced by the DBD plasma actuator. Due to laser reflection, the velocity profile near the delta wing surface could not be measured, and this area is left blank in Fig. 2. The streamlines reveal that the outboard air was sucked toward the leading edge, following which a jet tangential to the delta wing's leeward surface was formed. This is very similar to the ionic wind generated by using a flat-plate DBD plasma actuator.[12] The maximum ionic wind velocity was around 3.2 ms^{-1} and was located over the insulated electrode.

The flow structure in the transverse cross-section at the angle of attack $\alpha = 36°$ and $Re = 50\,000$ was illustrated by smoke flow visualization. In the baseline case, shown in Fig. 3(a), two "black lines" were visible in the middle of the areas occupied by the smoke, representing the LEV cores. Near the position of $x = 0.62\ c$, the cores suddenly expanded and then disappeared. This can be identified as the LEV breakdown locations. In Fig. 3(b), with the front pair of DBD plasma actuators ignited, the structures of the LEVs are significantly transformed: the shapes of the LEV cores are not as straight as those in the baseline case, and the LEV breakdown locations are delayed downstream by more than 0.1 c. When only the DBD on the starboard is ignited, as shown in Fig. 3(c), it is evident that the starboard LEV breakdown location is greatly advanced to 0.44 c, whereas that on the portside is delayed to far behind 0.9 c. The comparison between Figs. 3(b) and 3(c) reveals that the DBD plasma actuators in these two cases lead to opposite control effects on the starboard.

Figure 4 shows the PIV result in the spanwise perpendicular cross section at $x = 0.4\ c$ ($\alpha = 36°$; $Re = 50\,000$). The coordinates are normalized by the local semi-span length (S_L), and the vorticity is normalized as $\omega_x^\star = \omega_x c/U_\infty$. In the baseline case [Figs. 4(a) and 4(d)], the LEV cores are clearly identified by the highly concentrated vorticity in both the instantaneous and time-averaged vorticity contours. Around the LEV cores, several stationary vortical substructures are observed in the rolling-up shear layers. The velocity vectors show that the rolling-up shear flows, which originate from the leading edges, form a saddle point above the delta wing and a half-saddle point (the reattachment point) on the delta wing, marked by $\mathcal{S}$ and $\mathcal{HS}$ in Fig. 4(d), respectively.

Once both DBD plasma actuators are ignited [Figs. 4(b) and 4(e)], the rolling-up shear layers become markedly deformed and shift to the inboard sides, and the whole flow structure of the LEV is pushed down toward the delta wing surface. Consequently, the saddle point $\mathcal{S}$ is displaced from $z/S_L = 0.85$ to $z/S_L = 0.7$, and the time-averaged LEV cores are shifted from $z/S_L = 0.3$ to $z/S_L = 0.2$. The vortical substructures in the shear layers still exist [Fig. 4(b)]; however, they are unstable and circulate around the LEV cores, and so, no concentrated substructure exists in the time-averaged contour. Meanwhile, the strength of the LEVs is weakened compared with those in the baseline case.

When only the DBD plasma actuator on the starboard is powered [Figs. 4(c) and 4(f)], the change in the local flow structure on the starboard is very similar to that in the symmetric control case: the shear layer is deformed and shifted to the inboard side, and the LEV structure is pushed downward. Meanwhile, the vortical substructures continuously roll up and circulate around the LEV core. Notably, the vortex breakdown on the starboard is advanced to $x = 0.44\ c$ [Fig. 3(c)]. Therefore, at $x = 0.4\ c$, the LEV remains intact. On the portside, both the instantaneous and time-averaged

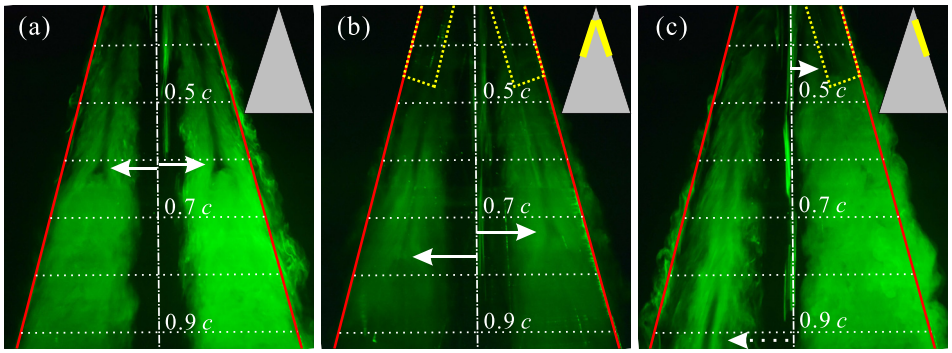

FIG. 3. Smoke flow visualization results show the typical LEV structure in the transverse cross-section: (a) baseline case; (b) symmetric control case; and (c) asymmetric control (starboard-controlled) case. ($\alpha = 36°$; $Re = 50\,000$).

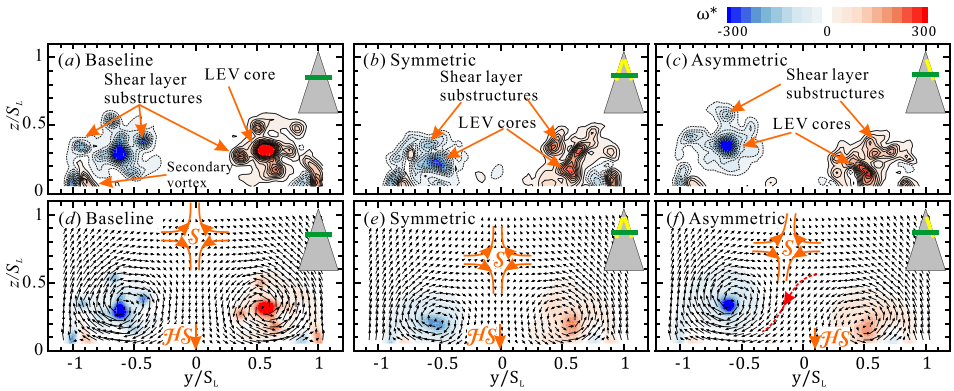

FIG. 4. PIV results showing the dimensionless vorticity contour $\omega_x^* = \omega_x c/U_\infty$ in the spanwise cross section at x = 0.4 c: (a) baseline case, (b) symmetric control case, and (c) asymmetric control (starboard) case; and the time-averaged velocity vectors and the dimensionless vorticity contour: (d) baseline case, (e) symmetric control case, and (f) asymmetric control (starboard) case ($\alpha = 36°$; $Re = 50\,000$).

vorticity contours show a highly concentrated LEV core, indicating that the portside LEV is strong and stable. The position of this LEV core is slightly lifted from $z/S_L = 0.3$ in the baseline case to $z/S_L = 0.35$. The time-averaged velocity vector clearly demonstrates that the saddle point $\mathcal{S}$ is pushed from the symmetric plane to the portside, whereas the half-saddle point $\mathcal{HS}$ is shifted to the starboard. Meanwhile, between these two critical points, part of the shear layer on the starboard crosses the symmetric plane and accompanies the shear layer on the portside [highlighted by the red dashed line in Fig. 3(f)], instead of rolling into the starboard LEV.

Therefore, Fig. 4 shows that the DBD plasma actuators affect the LEV systems by controlling the shear layer directly from the leading edges. A spanwise momentum (Fig. 2) is added into the rolling-up shear layer by the plasma actuator. Thus, the curvature of the shear layer is deformed, resulting in the unsteadiness of the shear layer's vortical substructures.[13] Even though the modifications induced by the control are very similar locally in the symmetric and asymmetric control cases, they lead to opposite control effects on the global flow structure [Figs. 4(b) and 4(c)]. The mechanism responsible for these opposite effects is the interaction between the pair of LEVs. In the symmetric control case, the interaction between the LEVs ensures that the whole structure remains symmetric. The displaced saddle point $\mathcal{S}$ leads to a contraction effect on the LEVs, which accelerates the longitudinal velocity and delays the vortex breakdown [Fig. 3(b)].[14] In the asymmetric control case, the interaction between the pair of LEVs transfers momentum from the starboard to the portside. Therefore, the loss of vorticity feeding from the shear layer leads to an earlier breakdown of the LEV on the starboard. Meanwhile, the portside LEV is strengthened and its breakdown location is delayed.

Figure 5(a) presents the lift coefficients (defined as $C_L = L/0.5\rho U_\infty^2 S$) as colored symbols and the estimated potential-flow lift coefficient,[15] $C_{L,P}$, as a dashed line. Hence, C_L-$C_{L,P}$ is the corresponding vortex lift. In the symmetric case, because of the weakened and displaced LEVs [Fig. 4(b)] and the delayed breakdown locations [Fig. 3(b)], the overall change in C_L is very small. In the asymmetric case, the loss of lift on the starboard caused by the advanced vortex breakdown location is almost equal to the enhancement of lift on the portside caused by the delayed vortex breakdown location so that C_L again remains almost unchanged. The drag coefficients, C_D, presented in Fig. 5(b) show similar tendencies to the lift coefficients for all cases.

As expected, the DBD plasma actuators induce relatively large changes in the moment coefficients (defined as $C_M = M/0.5\rho U_\infty^2 Sc$) of the delta wing, as shown in Fig. 5(c). In the symmetric case, the symmetry of the controlled LEV system ensures that the roll moment coefficient, $C_{M,R}$, is always around zero. The shift of the force center induces a change in the pitch moment, $C_{M,P}$. In the asymmetric case, the asymmetry of the flow structure leads to a large roll moment, as well as a change in the pitch moment. In response to the reduction of force, the pitch moment undergoes a relatively large change near the stall angle in the asymmetric case.

In summary, the mechanism by which DBD plasma actuators control the LEV breakdown over a delta wing was investigated experimentally. The results show that the DBD plasma actuators deform the shear layer from the leading edges, resulting in the transformation of the global structure: in the symmetric case, both breakdown locations are delayed,

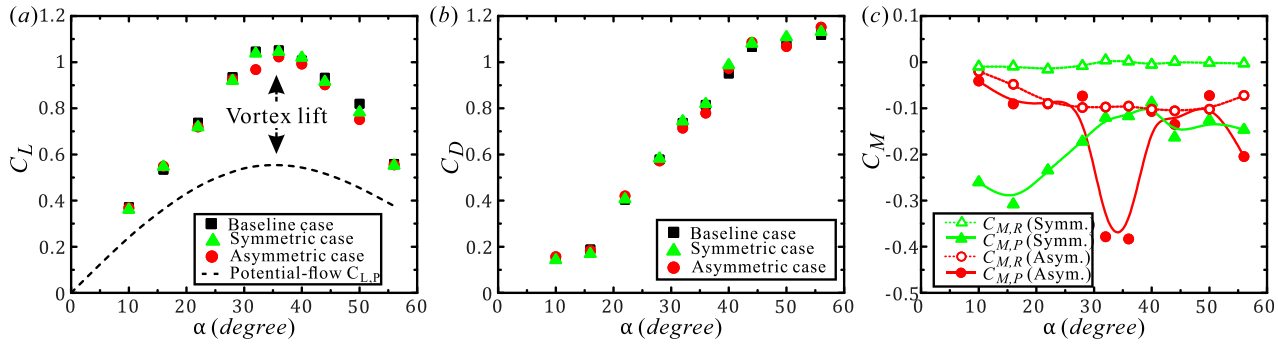

FIG. 5. (a) Lift coefficient C_L, (b) drag coefficient C_D, and (c) changes in the roll and pitch moment coefficient C_M plotted against the angle of attack α for the asymmetric case and the symmetric case ($Re = 50\,000$).

whereas in the asymmetric case, the breakdown location on the controlled semi-span is advanced while that on the non-controlled side is delayed. The interaction between the pair of LEVs is responsible for the opposite control effects on the controlled semi-span in these two cases, via the transfer of momentum through the two semi-spans. The aerodynamic response to the controls suggests that the DBD plasma actuator is a promising technique for delta wing maneuvering. Periodic control will be studied in the future to investigate the influence of actuating frequency on control authority, LEV stability, and control efficiency.

The authors would like to thank Hong Kong Research Grants Council (No. GRF526913), Hong Kong Innovation and Technology Commission (No. ITS/334/15FP), and the U.S. Office of Naval Research Global (monitored by Dr. Woei-min Lin, No. N62909-16-1-2161) for financial support.

[1]A. M. Mitchell and J. Delery, "Research into vortex breakdown control," Prog. Aerosp. Sci. **37**, 385–418 (2001).
[2]I. Gursul, Z. Wang, and E. Vardaki, "Review of flow control mechanisms of leading-edge vortices," Prog. Aerosp. Sci. **43**, 246–270 (2007).
[3]D. Greenblatt, B. Goksel, I. Rechenberg, C. Y. Schle, D. Romann, and C. O. Paschereit, "Dielectric barrier discharge flow control at very low flight Reynolds numbers," AIAA J. **46**, 1528–1541 (2008).
[4]F. O. Thomas, T. C. Corke, M. Iqbal, A. Kozlov, and D. Schatzman, "Optimization of dielectric barrier discharge plasma actuators for active aerodynamic flow control," AIAA J. **47**, 2169–2178 (2009).
[5]T. C. Corke, C. L. Enloe, and S. P. Wilkinson, "Dielectric barrier discharge plasma actuators for flow control," Annu. Rev. Fluid Mech. **42**, 505–529 (2010).
[6]J.-J. Wang, K.-S. Choi, L.-H. Feng, T. N. Jukes, and R. D. Whalley, "Recent developments in dbd plasma flow control," Prog. Aerosp. Sci. **62**, 52–78 (2013).
[7]M. P. Patel, T. T. Ng, S. Vasudevan, T. C. Corke, and C. He, "Plasma actuators for hingeless aerodynamic control of an unmanned air vehicle," J. Aircr. **44**, 1264–1274 (2007).
[8]D. Greenblatt, Y. Kastantin, C. N. Nayeri, and C. O. Paschereit, "Delta-wing flow control using dielectric barrier discharge actuators," AIAA J. **46**, 1554–1560 (2008).
[9]A. A. Sidorenko, A. D. Budovskiy, A. A. Maslov, B. V. Postnikov, B. Y. Zanin, I. D. Zverkov, and V. V. Kozlov, "Plasma control of vortex flow on a delta wing at high angles of attack," Exp. Fluids **54**, 1585 (2013).
[10]H. Du, Z. Shi, K. Cheng, D. Wei, Z. Li, D. Zhou, H. He, J. Yao, and C. He, "Topological structures of vortex flow on a flying wing aircraft, controlled by a nanosecond pulse discharge plasma actuator," Appl. Phys. Lett. **108**, 244105 (2016).
[11]L. Shen, C-y. Wen, and H.-A. Chen, "Asymmetric flow control on a delta wing with dielectric barrier discharge actuators," AIAA J. **54**, 652–658 (2016).
[12]E. Moreau, "Airflow control by non-thermal plasma actuators," J. Phys. D: Appl. Phys. **40**, 605–636 (2007).
[13]A. J. Riley and M. V. Lowson, "Development of a three-dimensional free shear layer," J. Fluid Mech. **369**, 49–89 (1998).
[14]M. Escudier, J. Bornstein, and N. Zehnder, "Observations and lda measurements of confined turbulent vortex flow," J. Fluid Mech. **98**, 49–63 (1980).
[15]E. C. Polhamus, "A concept of the vortex lift of sharp-edge delta wings based on a leading-edge-suction analogy," NASA Report No. TN-D-3767 (1966).